EFDA–JET–PR(08)44

A.V. Chankin, D.P. Coster, G. Corrigan, S.K. Erents, W. Fundamenski,
A. Kallenbach, K. Lackner, J. Neuhauser, R. Pitts, the ASDEX Upgrade Team
and JET-EFDA Contributors

Fluid Code Simulations of Radial Electric Field in the Scrape-Off Layer of JET

Fluid Code Simulations of Radial Electric Field in the Scrape-Off Layer of JET

A.V. Chankin[1], D.P. Coster[1], G. Corrigan[2], S.K. Erents[2], W. Fundamenski[2], A. Kallenbach[1], K. Lackner[1], J. Neuhauser[1], R. Pitts[3], the ASDEX Upgrade Team and JET-EFDA Contributors*

JET-EFDA, Culham Science Centre, OX14 3DB, Abingdon, UK

[1]Max-Planck-Institut für Plasmaphysik, EURATOM Association, Garching, Germany
[2]EURATOM-UKAEA Fusion Association, Culham Science Centre, Abingdon, UK
[3]Centre de Recherches en Physique des plasmas, Association EURATOM-Confédération Suisse, École Polytechnique Fédérale de Lausanne, Ch-1015, Switzerland
** See annex of F. Romanelli et al, "Overview of JET Results", (Proc. 22 nd IAEA Fusion Energy Conference, Geneva, Switzerland (2008)).*

Preprint of Paper to be submitted for publication in
Plasma Physics and Cotrolled Fusion

ABSTRACT.

Recent simulations of JET and ASDEX Upgrade plasmas with EDGE2D and SOLPS, respectively, showed that upstream radial electric field in the Scrape-Off Layer (SOL) is substantially below values expected from simple estimates, based on the effects of the potential Debye sheath drop at the target and thermoelectric force. This served as a motivation for the dedicated EDGE2D-Nimbus modelling of JET plasmas aimed at identification of key mechanisms responsible for the formation of the radial electric field (E_r) in the main SOL of high recycling divertor plasmas. Code runs with different upstream density and input power levels were carried out, aimed at obtaining both 'cold' (with flat outer target electron temperature, T_e, profiles and low peak T_e values, compared to the upstream ones) and 'hot' (with peaked outer target T_e profiles and the maximum target T_e values comparable to the upstream ones) divertor solutions.

It was found that in 'cold' divertor solutions, the contribution of target Debye sheath drops to the formation of the upstream E_r is small, as expected. Under such conditions, other contributions, originating from the parallel electron force balance, become important. The two main contributions: from the thermoelectric force ($-0.71\nabla_{||}T_e$, for singly charged ions), and parallel electron pressure gradient ($-\nabla_{||}p_e/n_e$), were found, however, to counteract each other, reducing the upstream E_r. In 'hot' divertor solutions, the Debye sheath mechanism is more important, but it is partly compensated by the (radial) profile effects of the increased $-\nabla_{||}p_e/n_e$ contribution (p_e and n_e–electron pressure and density). The latter is related to the formation of a local maximum of p_e around the X-point position on flux surfaces close to the separatrix and is attributed to ionization of neutrals.

INTRODUCTION

From the simple Scrape-Off Layer (SOL) model with no neutral recycling and poloidally constant electron temperature T_e, one expects positive radial electric field $E_r \equiv -\nabla_r V_p$ (V_p is plasma potential) of order $-3\nabla_r T_e/e$, with e being charge of electron (see e.g. [1], p. 543). This result is easily obtained by assuming ambipolar plasma flow to the electrically conducting target and Debye sheath drop of electric potential ~$3T_e/e$ at the target surface. In strongly recycling divertor plasmas realized in today's tokamaks with fairly closed divertors, and also envisaged for the ITER operation [2], E_r in the 'main SOL', upstream of the divertor (along the field lines), should be lower. Normalized to the local T_e gradient taken with the opposite sign (resulting in the dimensionless ratio $-eE_r/\nabla_r T_e$), it is expected to be substantially below 3 due to the temperature drop towards the target. Provided the target T_e is significantly below the upstream value, measured e.g. at the outer midplane position, $T_{e,tar} << T_{e,mid}$, the Debye sheath contribution to the upstream E_r almost vanishes and its value is determined by secondary mechanisms arising from the *parallel* electron force balance equation: parallel electron pressure gradient $\nabla_{||}p_e$,, parallel electron thermoelectric force ($-0.71n_e\nabla_{||}T_e$, for singly charged ions [3]), and parallel thermoelectric currents [4] (currents flowing between the two targets and caused by the difference in their Debye sheath potentials due to the difference in target T_e). All these contributions are analysed in the present paper with the aim of establishing key

mechanisms contributing to the E_r formation in the 'main SOL', far away from the divertor, under different divertor conditions.

A particular interest in clarifying mechanisms contributing to the E_r formation in the SOL is sparked by recent findings that 2D fluid code simulations tend to underestimate experimentally measured E_r in the SOL. This was established by comparing ASDEX Upgrade (AUG) data with SOLPS code simulations and JET data–with EDGE2D code simulations [5]. In addition, the tendency for the codes to underestimate parallel ion flows in the SOL (see e.g. [6, 7]) and divertor T_e (thereby *overestimating* its electron density n_e, for the same parallel heat flux density, see refs. inside [5]) was also established. All these discrepancies raise the question about the validity of fluid codes for the plasma edge modelling. 2D fluid codes simulate experimental conditions using parallel equations for plasma species that assume strong collisionality. Guiding centre drift motions are also usually included in the plasma equations. The neutral species behaviour and their interaction with the plasma are usually modelled with Monte-Carlo simulations of all known chains of reactions involving atoms and molecules. Perpendicular plasma transport, at the same time, is described by ad-hoc transport coefficients that allow the modeller to match various experimental profiles in either SOL or the divertor. Fluctuations of plasma parameters existing in real turbulent plasmas are ignored. Also ignored are kinetic effects of the parallel plasma transport. It would be natural therefore to attribute the discrepancies between the codes and experiment to either the influence of fluctuations on averaged plasma parameters, or to kinetic effects. For example, it is well known that electrons responsible for the bulk of the parallel heat conduction from the upstream SOL to the divertor under typical experimental conditions are only very weakly collisional, see e.g. [8, 9, 5]).

The main purpose of the present paper is to identify basic mechanisms contributing to the E_r formation in the SOL using known physics included in the present day 2D fluid codes. Discrepancies with experimental results, indicative of the role of unaccounted effects in the codes, will be touched upon only briefly. Part of the motivation for the present work was also to check the code results on the internal self-consistency, and to qualitatively understand the code results on the E_r profiles in the SOL.

'Hot' and 'cold' divertor solutions

As was already pointed out in the Introduction, the contribution of the Debye sheath to the E_r in the SOL strongly depends on the T_e profile at the target(s). The ratio $-eE_r/\nabla_r T_e$, where both parameters are taken upstream (usually at the outer midplane position) should be particularly sensitive to the ratio of the target to upstream T_e. The latter mainly depends on the recycling in the divertor and the balance between particle and power fluxes in the divertor/SOL. One can then speak of 'hot' or 'cold' divertor conditions (or code solutions) depending on whether the ratio $T_{e,tar}/T_{e,mid}$ is ~ 1 or $\ll 1$, respectively. As will be shown below, relative weight of other mechanisms contributing to the E_r, apart from the Debye sheath, also depends on the divertor conditions.

The 2D fluid codes, as was mentioned above, tend to predict 'colder' (with lower T_e) and 'denser' (with higher n_e) plasmas in the divertor compared with the experiment, for typical discharge conditions with medium densities (for very low densities, when recycling in the divertor is strongly reduced, SOLPS modelling of AUG plasmas shows that the peak target T_e becomes comparable to the outer midplane T_e, hence, a 'hot' solution correctly describing the experiment can be obtained [10]). For 'cold' divertor solutions, not only the maximum value of T_e at the targets, $T_{e,max}$, is much lower, but also it is obtained further away from the strike point (the target T_e usually rises from the separatrix/strike point deeper into the SOL, reaches its maximum and then decays), and the target T_e profiles are generally flatter than in 'hot' divertor solutions. This leads to a fairly low upstream E_r. A comparison between experimentally measured E_r in JET and AUG with EDGE2D and SOLPS solutions, respectively, for typical Ohmic and H-mode conditions in both machines, shows that the $-eE_r/\nabla_r T_e$ ratios in the codes are around zero, and in any case don't exceed ≈ 0.5 [5]. At the same time, experimental values obtained with reciprocating Langmuir probes give an average value of $\approx$ 1.6 for JET (for regimes of various confinement properties) and ≈ 3 for a medium density Ohmic shot of AUG. Reasons why in some experiments measured $-eE_r/\nabla_r T_e$ ratios can be close to or even above 3 (the maximum predicted value that would follow from the simple SOL model using Debye sheath arguments), are likely to be related to unaccounted effects in 2D fluid codes and are not discussed in the present paper. The main task here is to explain why the code $-eE_r/\nabla_r T_e$ ratios in 'cold' divertor solutions don't usually reach values ≈ 0.7 that could be expected from the parallel thermoelectric force, and why this ratio cannot be raised above ≈ 1 even at very low plasma densities.

By reducing plasma density in the SOL (a good figure of merit for the SOL density is usually the separatrix electron density at the outer midplane, n_s) for the same input power P_{in} into the numerical grid, or by increasing P_{in} keeping the same n_s, the divertor solution can be transitioned from the 'cold' to 'hot'. In the latter case, not only the ratio $T_{e,tar}/T_{e,mid}$ significantly rises across the profile, but also the maximum target T_e value $T_{e,max}$ shifts closer to the separatrix/strike point and the T_e profile becomes more peaked. In most of the SOL, the target T_e profile is decaying (in the direction away from the separatrix) and positive $-eE_r/\nabla_r T_e$ ratios are obtained, as expected. These ratios however are still below those that could be expected from the combined contribution of the Debye sheath and the parallel thermoelectric force. The reason for this is explained in the following sections.

Apart from the balance between input power and plasma density, a number of other factors can determine whether a solution in the divertor will be 'cold' or 'hot'. In the case of an open divertor (from which the recycled neutrals can easily escape without being ionized), easier access to the 'hot' divertor regime is achieved. Configurations with limiters, instead of divertors, also tend to provide 'hotter' solutions. Even for the same divertor geometry and magnetic configuration, a code solution with hydrogen as a working gas, instead of deuterium, is expected to be 'hotter' due to the increased mobility of neutrals for the same plasma and wall temperatures. Running cases with larger chemical sputtering coefficients, through the increase in the radiated power, also tends to make the divertor plasma 'colder'. Finally, a code solution for the divertor will depend on what

assumptions are used to describe the neutrals behaviour. For example, treating neutrals as atoms according to a fluid model may result in a 'hotter' divertor solution than using a Monte-Carlo code that also includes slow molecules and all chains of their break-up mechanisms (see e.g. [11] for an example of a relatively 'hot' SOLPS solution for the standard Ohmic AUG shot).

In the present paper, only closed divertor solutions with high recycling of neutrals and a large drop of T_e towards the target are considered. Such solutions are usually realized in divertor JET and AUG discharges and are also envisaged for ITER operation [13]. The modelling described here is based on EDGE2D cases simulating JET discharges, somewhat extended in parameter range in order to cover extreme cases of very low and very high densities (consequently, simulating distinct 'hot' and 'cold' conditions in the divertor).

SETUP OF EDGE2D RUNS

EDGE2D code simulations were carried out at various density and input power levels, in order to establish the most basic features of the E_r formation in the SOL for a wide range of plasma upstream collisionality, and simulating conditions of both 'hot' and 'cold' divertors. The basic modelling set-up for the coupled EDGE2D-Nimbus (the latter being the Monte Carlo code for neutrals) code runs simulating JET plasmas is described in [6]. As a prototype, low density Ohmic case for the JET Pulse No: 56723 in normal toroidal field (B_t) configuration (with ion ∇B drift towards the divertor) matching fairly well both upstream (from the divertor, along field lines) and target n_e and T_e profiles was selected. This case has an input power into the grid of 1.6MW, a 1:0.6 partition of power between ion and electron channels, toroidal field $B_t = 2T$ and plasma current $I_p = 2MA$. Compared to the original cases, which were run on a numerical grid with 8 rings in the core region, 4 – in the private region and 16 – in the SOL, the numerical grid was extended to include 16 rings in both core and SOL, and 8 – in the private region. Drifts were switched on everywhere across the grid, compared to the original cases where they were only switched on in the SOL. Original transport coefficients were used: particle perpendicular diffusion coefficient $D_\perp = 0.5\ m^2s^{-1}$, except for the region in the SOL between 1.6 and 2.8 cm (mapped to the outer midplane position) where $D_\perp$ is raised up to 1.5 m^2s^{-1}, and ion and electron perpendicular heat conductivities $\chi_i = \chi_e = 3\ D_\perp$. In the private region, coefficients $D_\perp \approx 0.6\ m^2s^{-1}$ and $\chi_i = \chi_e = 0.15 – 2\ m^2s^{-1}$ were used.

The same numerical grid was used for reversed B_t cases (with ion ∇B drift away from the divertor) as for normal B_t cases, in difference to the modelling described in [6], where slightly different grids were used for real JET pulses with opposite B_t directions. The density control was also slightly modified in order to ensure that exactly the same separatrix electron density n_s is achieved in normal and reversed B_t configurations. Separatrix density n_s was maintained by a feedback loop using adjustable recycling at targets and walls, in the presence of a constant and poloidally uniform gas puffing of $3\times10^{21}\ s^{-1}$, small core fuelling ($2.5\times10^{20}\ s^{-1}$) and pumping (the 'puff + recycling' option in EDGE2D). The chemical sputtering multiplier was set at 0.5, the same as in the original cases (see [6] for details).

With the above setup, a number of steady-state converged solutions were obtained for various density levels. In the normal B_t case with $n_s = 6.5\times10^{18}$ m^{-3}, target n_e and T_e profiles matched very well those of the original case. Profiles in the SOL were also very well matched, with the only exception being the peak value of the Mach number of the parallel ion flow that was by a factor of 1.3 larger (apparently due to drifts being switched on everywhere across the grid, compared to original cases, see above). Numerical stabilities of the code runs with drifts, however, restricted the available density range from both higher and lower boundaries. One of the lowest density cases had $n_s = 4\times10^{18}$ m^{-3} (the case with $n_s = 3.5\times10^{18}$ m^{-3} already collapsed), and one of the highest – $n_s = 8.5\times10^{18}$ m^{-3} (the case with $n_s = 9\times10^{18}$ m^{-3} collapsed).

At higher input power levels the above cases also suffered from numerical instabilities. The highest possible input power for a stable run was P_{in} = 6MW. A pair of cases at this power level, with the 2:1 partition of power between ions and electrons, and $n_s = 5\times10^{18}$ m^{-3} was chosen as representing L-mode conditions (referred to as 'L-mode' below). At even higher P_{in}, all cases using the fine numerical grid collapsed. An attempt to build H-mode cases with P_{in} above 7 MW using the numerical grid and other settings previously used in time-dependent JET ELMy H-mode non-drift simulations described in [12] have also collapsed due to numerical instabilities. As a representative of JET H-mode plasmas, one of the normal B_t cases on a rather coarse mesh around the separatrix described in [13] was chosen. This case had the same transport coefficients as Ohmic cases described above, input power of 12MW with the 2:1 partition between ions and electrons, $n_s = 1.1\times10^{19}$ m^{-3}, B_t/I_p = 2.4T/2.5MA. In the present work, this case was continued with the reversed B_t direction until it reached the new steady-state. Since separatrix density was fixed in these runs, the reversed B_t case was the direct counterpart of the original normal B_t case.

In total, 5 representative pairs (in normal and reversed B_t configurations) of JET cases were selected for detailed analysis: three Ohmic pairs with $n_s = 4\times10^{18}$, 6.5×10^{18} and 8.5×10^{18} m^{-3}, one L-mode pair, and one H-mode pair with a different numerical grid.

MODELLING RESULTS

Out of 5 pairs of cases selected, 2 can be qualified as having 'cold' divertor solutions (Ohmic cases with $n_s = 6.5\times10^{18}$ and 8.5×10^{18} m^{-3}) and 2 – 'hot' solutions (Ohmic cases with $n_s = 4\times10^{18}$ m^{-3} and L-mode cases with 5×10^{18} m^{-3}). The H-mode cases had a rather poor spatial resolution of the numerical grid around the separatrix position, and a well resolved peak in the T_e profile could not be seen. Comments about this case will be made near the end of this section.

The original, prototype case, as pointed out above, corresponds to an Ohmic JET Pulse No: 56723 in normal B_t configuration, simulated by the EDGE2D run with the input power into the grid of 1.6 MW and separatrix density $n_s = 6.5\times10^{18}$ m^{-3}. Code results for this case that matched fairly well both experimental upstream and target n_e and T_e profiles are presented in Fig.1. Except for very low density cases, the simulated target T_e profile doesn't usually show a clear peak near the strike point (the same applies to SOLPS cases modelling AUG plasmas [5]). This leads to fairly flat

outer target and outer midplane V_p profiles across most of the SOL, as can be seen from Fig. 1(left), and implying a rather small radial electric field $E_r \equiv -\nabla_r V_p$. The connection between the target plasma potential and T_e, as pointed out in the Introduction, is mainly determined by the Debye sheath drop ~ $3T_e/e$, but is also affected by the current density to the target (see below). The target potential propagates along the field lines to the outer midplane. However, three extra contributions accumulated along field lines arise. They follow from the parallel force balance equation for electrons (coefficient 0.71 is correct for singly charged ions, but rises up to 1.5 in the limit of $Z_i = \infty$) [3]:

$$E_{||} = -0.71\nabla_{||} T_e/e - \nabla_{||} p_e/en_e + j_{||}/\sigma_{||} \quad (1)$$

Fig. 1(right) shows the difference between the outer midplane and outer target potential energies and its break-up into individual components, according to Eq. (1). Actual values of Z_{eff} predicted by the code were used to calculate the coefficients before the $\nabla_{||} T_e/e$ term as well as for the calculation of the parallel conductivity $\sigma_{||}$. As one can see, in almost all the first half of the SOL, adjacent to the separatrix, profile effects of the thermoelectric force ~ $\nabla_{||} T_e$ (marked 'temp. grad. force' on the figure) and pressure-gradient force $\nabla_{||} p_e/n_e$ nearly cancel each other out, resulting in a rather flat outer midplane V_p profile. The integrated friction force $ej_{||}/\sigma_{||}$ doesn't contribute much to the upstream potential profile; further comments on its magnitude and direction will be made later in this section.

A non-homogeneity seen in both the ($eV_{p\ midp.} - eV_{p\ tar.}$) and integrated $\nabla_{||} p_e/n_e$ profiles at the first 2 rings outside of the separatrix, is real and is not the result of some numerical instabilities of the solution. The existence of such features depends on the particularities of parallel T_e and n_e profiles between the outer target and the outer midplane. The large negative value of the integrated $\nabla_{||} p_e/n_e$ term on the 1st ring outside of the separatrix is caused by a large build-up of plasma density near the X-point position, combined with a rather low T_e from the outer target up to the X-point. Due to very low T_e (less than 5eV along most of the distance), this region doesn't contribute much to the integrated $\nabla_{||} p_e/n_e$ term. Near the X-point, T_e sharply rises while n_e sharply drops. The effect of the latter is stronger than that of the former, resulting in a large negative contribution to the integrated $\nabla_{||} p_e/n_e$ term which determines its overall negative sign. On the 2nd ring, in difference to the situation on the 1st ring, there is a certain p_e rise from the X-point to the outer midplane. In this region, the T_e is already fairly high and n_e – low, resulting in a large positive contribution to the integrated $\nabla_{||} p_e/n_e$.

For the same case, but in the reversed B_t configuration, instead of a drop, an increase in the integrated $\nabla_{||} p_e/n_e$ term on the 1st ring outside of the separatrix can be seen (see Fig.2).

Across all cases, the tendency towards reversing the parallel ion flow near the divertor from being directed towards the target is seen. It is related to the 2D effect of higher rates of neutral ionization near the separatrix where both plasma density and upstream T_e (hence, larger parallel electron heat flux towards the X-point region and divertor sustaining higher local T_e) are higher, leading to a further increase in p_e. The peaks in p_e, reached usually in between the target and the X-

point position, tend to drive the plasma away from the divertor into the main SOL, a phenomenon known as the 'ionization-driven flow reversal' (see e.g. original papers [14-17], also Stangeby's book [1], pp. 471-476, and a review paper [18], pp. R212-R216). The total plasma pressure including kinetic ( ) and viscous parts, is also larger at the target than upstream. The flow reversal tends to be stronger at lower densities, while disappearing at very high densities when the plasma goes into the detachment in the divertor. It can occur in both outer and inner divertor legs and is more easily achieved in divertor configurations with vertical rather than horizontal targets. One example of vector plots showing the 2D distribution of the parallel ion Mach number in the divertor will be presented later in this section.

Associated with the appearance of peaked parallel p_e profiles (that lead to the flow reversal at lower plasma densities), is the drop in the integrated $\nabla_{||} p_e/n_e$ term closer to the separatrix in the SOL. Without such a peak in the electron pressure, there would be a usual pressure drop towards the target related to the acceleration of the plasma up to the local ion sound speed as seen in the outer SOL, hence, a positive integrated $\nabla_{||} p_e/n_e$ term. The drop in this term towards the separatrix is the main reason for very low SOL E_r in 'cold' divertor solutions. In 'hot' solution, it limits the rise of the E_r that could be achieved due to Debye sheath contributions in the presence of target T_e comparable to the upstream values and peaked target T_e profiles, as will be shown below. A very high correlation between overall ($eV_{p\ midp.} - eV_{p\ tar.}$) profiles and their local features, on the one hand, and profiles of the integrated $\nabla_{||} p_e/n_e$ term seen in all EDGE2D solutions (see more examples below) shows the significance of this term in the formation of the E_r in the SOL.

The signs of the integrated friction force $ej_{||}/\sigma_{||}$ in the normal and reversed B_t cases shown in Figs. 1 and 2 are consistent with the signs of current densities to the targets: negative 'friction force' implies negative current density to the outer target (and positive – to the inner target). Currents flowing from the outer to inner target in normal B_t plasmas, and - in the opposite direction in reversed B_t plasmas, are often referred to as thermoelectric currents driven by the difference between Debye sheaths between the two targets caused by the asymmetry in the target T_e [4]. Note however that, consistent with observations in many experiments, the strong target temperature asymmetry in favour of the outer target in the normal B_t case shown in Fig.1 is not reversed, but only reduced, when the field is reversed (Fig.2), in contrast to the parallel currents that usually do reverse (see e.g. [19]). The simple thermoelectric current therefore can't explain the direction of the parallel current, and other drivers for the parallel current density, apart from the difference between plasma potentials near the targets, should be considered. Their relative contribution increases as target T_e are reduced, which for the cases shown in Figs. 1 and 2 is near the separatrix, and the prediction of the direction of the parallel current becomes non-trivial. The equation for the parallel current density is obtained by integrating Eq. (1) along the field line from one target to the other, with the replacement of $\int E_{||} ds_{||}$ by the potential difference between the targets and the inclusion of target boundary conditions for the parallel currents (see equations for the parallel current implemented in EDGE2D in [20]).

Below, three more examples of the same profiles for various cases are presented, only for normal B_t configurations. EDGE2D results for an Ohmic case with one of the highest possible densities (without causing a numerical instability), $n_s = 8.5\times10^{18}$ m^{-3}, are presented in Fig. 3. The trends are essentially the same as for the previous normal B_t case. The upstream electric potential profile is rather flat, implying nearly zero E_r, owing to very low target T_e (hence, small Debye sheath drops), and almost complete compensation of the thermoelectric force by the $\nabla_{\|}p_e/n_e$ force. The relative contribution from the thermoelectric force is lower than in the previous case due to lower target T_e in the plasma.

In order to obtain positive upstream E_r, an Ohmic case with an extremely low separatrix density, $n_s = 4\times10^{18}$ m^{-3}, was run. The results are presented in Fig.4. At the outer target, the T_e profile is now well peaked, with the maximum value being almost a half of the upstream T_e. Due to the contribution from the Debye sheath at the outer target, a positive E_r throughout most of the SOL is formed. The upstream E_r rise near the separatrix, however, is limited, and doesn't reflect the full extent of the E_r rise near the target. The main reason for this is the large p_e increase near the strike point, sufficient to force parallel plasma flow away from the target in the divertor ('flow reversal') in this case. A very good spatial correlation between ($eV_{p\ midp.} - eV_{p\ tar.}$) and its integrated $\nabla_{\|}p_e/n_e$ contribution can be seen, confirming the leading role of this contribution in limiting the increase in the upstream E_r. The outer midplane and outer target E_r, as well as radial gradients of T_e at these positions, are plotted in Fig. 5 for the same case. The outer midplane E_r is below that at the outer target near the separatrix, except for the innermost point. The ratio $-eE_r/\nabla T_e$ at the outer midplane is ≈ 1 for most of the SOL, but drops towards the separatrix.

The contour plot of electron pressure for the low density Ohmic case in normal B_t configuration, with the results presented in Fig.1, is shown in Fig.6. A wide region of high p_e exceeding 3×10^{20} m^{-3}eV, protruding into the outer divertor plasma from the core, with the peak value above 3.5×10^{20} m^{-3}eV, can be seen in the figure, marked by the near horizontal arrow. In addition, a few local peaks reaching, or exceeding, the 3×10^{20} m^{-3}eV level, are also shown by arrows.

Vector plots of the Mach number of the parallel ion flow in and around the divertor for the same case are shown in Fig.7. The figure on the right shows the expanded view of the square area marked by dashed lines on the left figure. A flow reversal, from around the X-point position upstream, can be clearly seen on the 1st ring outside of the separatrix. It is also present on the 2nd ring, but the absolute Mach numbers there are almost negligible.

Finally, results for the case with $n_s = 5\times10^{18}$ m^{-3} and an increased input power of 6MW, which would correspond to an L-mode discharge of JET, are presented in Fig. 8. The trends are essentially the same as for the lowest density Ohmic case, but are even more pronounced. Due to the increased T_e at the outer target, the difference between plasma potentials near the two targets drives a uni-directional current from the outer target to the inner, and the contribution of the friction force to the difference ($eV_{p\ midp.} - eV_{p\ tar.}$) becomes significant. This case, as well as the previous one, are typical examples of 'hot' solutions for the SOL and divertor, with fairly peaked (outer) target T_e profiles, while the examples before represented 'cold' solutions.

As was pointed out in the previous section, H-mode input parameters presented significant numerical problems for running EDGE2D cases with drifts. The available successful runs with high input power (12MW) described in [13] (but not shown here), at the same time, have a rather course numerical grid near the separatrix in the SOL. The peak target T_e is therefore more difficult to determine. It is above 40eV, with the separatix $T_e \approx 120$eV. Judging by the profiles of ($eV_{p\ midp.} - eV_{p\ tar.}$) and the integrated $\nabla_{||} p_e/n_e$ contribution (both go to very low negative values), these are typical 'hot' solutions. The outer midplane plasma potential profiles, for both normal and reversed B_t cases, show only relatively small variations, confirming low upstream E_r in the SOL.

SUMMARY

EDGE2D modelling of configurations with the high recycling JET divertor identified mechanisms responsible for the formation of the radial electric field in the scrape-off layer. Large $E_r \sim -3\nabla_r T_e/e$ following from the simple SOL model are not achieved in any of the code solutions. In high density plasmas (and moderate input power) 'cold' divertor solutions are realized, with flat target T_e profiles, low peak T_e and correspondingly small Debye sheath drops at the target. Under such conditions, the upstream E_r is determined by other contributions (rather than from the target Debye sheath drops) that would have otherwise been considered of secondary importance. The most important of these contributions are parallel thermoelectric force ($-0.71 n_e \nabla_{||} T_e$, for singly charged ions) and electron pressure-gradient force $-\nabla_{||} p_e$. They influence the upstream electric potential via parallel integrals of $-0.71\nabla_{||} T_e/e$ and $-\nabla_{||} p_e/n_e e$, respectively. *Radial* gradients of these *parallel* contributions to the potential difference ($V_{p\ midp.} - V_{p\ tar.}$) are mainly responsible for the formation of the upstream E_r.

In 'cold' divertor solutions, the radial variation of the contribution from the thermoelectric force is largely balanced by that from the $-\nabla_{||} p_e/n_e e$ term, resulting in a rather flat upstream potential profile with very small $E_r << \nabla_r T_e/e$. The contribution to the upstream E_r from the friction force (due to the parallel current) was found to be relatively small. By reducing density in the SOL or increasing the input power, a 'hot' divertor solution can be obtained, with the peaked target T_e profile (usually – at the outer target in normal B_t configurations, but can also be at both targets in reversed B_t configurations) and a more significant contribution from the Debye sheath potential drops. The rise in the upstream E_r under these conditions is nevertheless limited, and is typically below $\nabla_r T_e/e$. Near the separatrix, the E_r sharply drops due to the increased contribution from the -$\nabla_{||} p_e/n_e e$ term.

For all EDGE2D solutions analysed, the electron pressure at the outer midplane was greater than that at the outer target. This is in a sharp contrast with the integral of $\nabla_{||} p_e/n_e$ which is positive only in the outer SOL. This integral is strongly reduced in the near SOL and typically becomes negative near the separatrix. Such a behaviour is a consequence of peculiarities in the parallel n_e and T_e profiles caused by the strong ionization source. In the outer SOL, the contribution from neutral ionization to the parallel force balance is relatively small, and the electric potential shows a drop towards the target plate due to the usual pressure drop associated with the acceleration of the

plasma up to the local ion sound speed. In contrast, in the near SOL, strong ionization source creates a local maximum in the p_e around the X-point position, and the distribution of n_e and T_e along the field lines is such that the integral of $\nabla_{\|} p_e/n_e$ can be negative. The spatial variation of this integral across the SOL acts so as to reduce the upstream E_r. The change of sign of the $\nabla_{\|} p_e/n_e$ integral near the separatrix position is closely associated with the well known phenomenon of the ionization-driven flow reversal. The formation of the local maximum in $(p_e + p_i)$ near the X-point can force the plasma to flow from the divertor into the main SOL region along the field lines.

It is important to note that real experimental E_r values in the SOL can diverge strongly from the EDGE2D and other fluid code predictions. In addition to the mechanisms analysed in this paper, there exist also other effects, not covered by the present day 2D fluid codes, as pointed out in the Introduction.

ACKNOWLEDGEMENTS

This work, supported by the European Communities under the contract of Association between EURATOM, Max-Planck-Institut für Plasmaphysik (Germany), and Centre de Recherches en Physique des plasmas (Switzerland), was carried out within the framework of the European Fusion Development Agreement. The views and opinions expressed herein do not necessarily reflect those of the European Commission.

REFERENCES

[1]. Stangeby P.C, in *The Boundary of Magnetic Fusion Devices*, IOP Publishing, Bristol (2000).

[2]. Loarte A, Lipschultz B, Kukushkin A.S , et al., Nucl. Fusion **47** (2007) S203-S263.

[3]. Braginskii S I, in *Reviews of Plasma Physics*, edited by M.A.Leontovich (Consultants Bureau, New York, 1965), Vol. 1, p. 205.

[4]. Harbour P.J, Contrib. Plasma Phys. **28** (1988) 4/5 417.

[5]. Chankin A.V, Coster D.P, Asakura N, et al., Nucl. Fusion **47** (2007) 479.

[6]. Erents S.K, Pitts R.A, Fundamenski W, et al., Plasma Phys. Control. Fusion 46 (2004) 1757.

[7]. Chankin A.V, Coster D.P, Asakura A, et al., Nucl. Fusion **47** (2007) 762.

[8]. Batishchev O.V, Krasheninnikov S.I, Catto Peter J, et al., Phys. Plasmas **4** (1997) 1672.

[9]. Chodura R., Contrib. Plasma Phys. **28** (1998) 4/5 303.

[10]. Wischmeier M, Bonnin X, Coster D, et al., 'Simulating the role of intrinsic impurities in the divertor detachment of ASDEX Upgrade', presented at *11th International Workshop on Plasma Edge Theory in Fusion Devices*, 23-25 May 2007, Takayama-city, Japan, paper P3-03, submitted for publication in Contrib. Plasma Phys.

[11]. Coster D.P, Chankin A V, Conway G D, et al., proc. of 32nd EPS Conference on Plasma Phys., Tarragona, 27 June – 1 July 2005 ECA Vol.29C, P-1.008 (2005).

[12]. Kallenbach A., Andrew Y., Beurskens M., Corrigan G., Eich T., et al., Plasma Phys. Control. Fusion **46** (2004) 431.

[13]. Erents S.K, Fundamenski W, Corrigan G, Matthews G.F, Zagorski R and EFDA-JET Contributors, J. Nucl. Mater. **363-365** (2007) 565.
[14]. Krasheninnikov S.I, Nucl. Fusion **32** (1992) 1927.
[15]. Maddison G.P, Reiter D, Stangeby P C and Prinja A K, 1993 *Proc. 20th EPS Conf. on Controlled Fusion and Plasma Phys.*, Lisboa, July 26-30, PII-779 (1993).
[16]. LaBombard B, Goetz J, Hutchinson I, et al., J.Nucl. Mater. **241-243** (1997) 149.
[17]. Boedo J.A, Porter G.D, Schaffer M J, et al., 1998 *Proc. 2t th EPS Conf. on Controlled Fusion and Plasma Phys.*, Praha, 29 June - 3 July 1998 ECA Vol. 22C, p.822 (1998).
[18]. Loarte A, Plasma Phys. Control. Fusion **43** (2001).
[19]. Chankin A.V, J. Nucl. Mater. **241-243** (1997) 199.
[20]. Radford G.J, Chankin A.V, Corrigan G, Simonini R, Spence J, Taroni A, Contrib. Plasma Phys. **36** (1996) 2/3 187

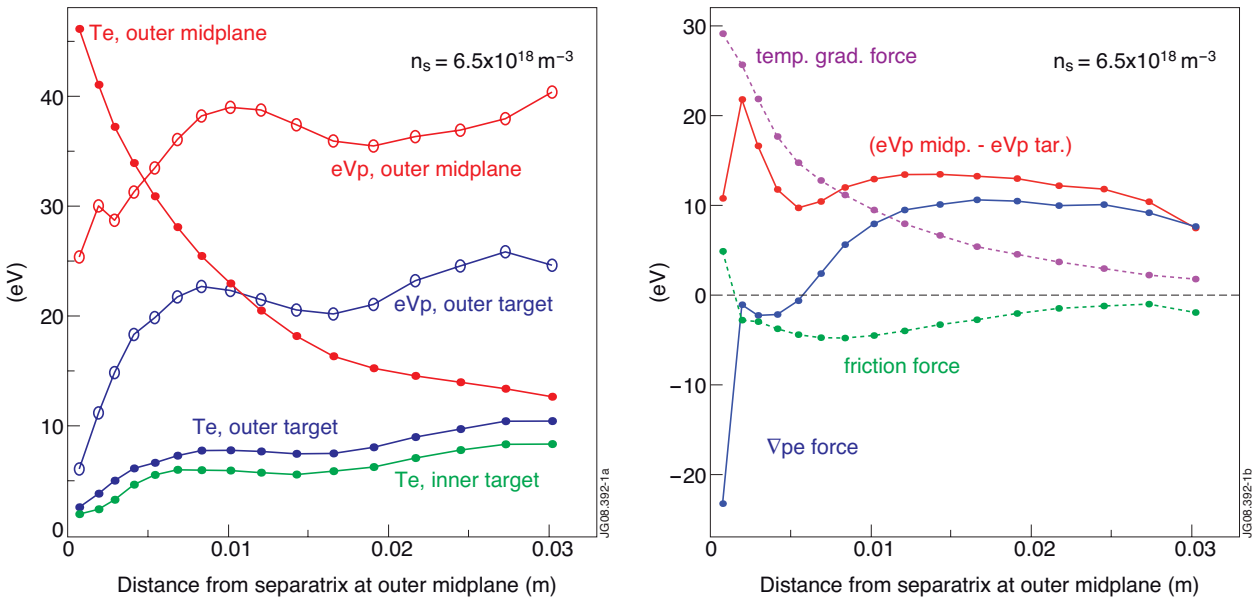

Figure 1: T_e and plasma potential V_p (multiplied by elementary charge e) at the outer midplane and outer target, and T_e at the inner target (left); the difference between outer midplane and outer target eV_p and its contributions: integrated friction force $ej_{//}/s_{//}$, integrated temperature gradient force ≈ $-0.71\nabla_{||}T_e$,, and integrated pressure gradient force $-\nabla_{||}p_e/n_e$ (marked as "$-\nabla p_e$ force" (right), for an Ohmic JET case with $n_s = 6.5\times10^{18} m^{-3}$ in normal B_t configuration. The distance from the separatrix is mapped to the outer midplane position.

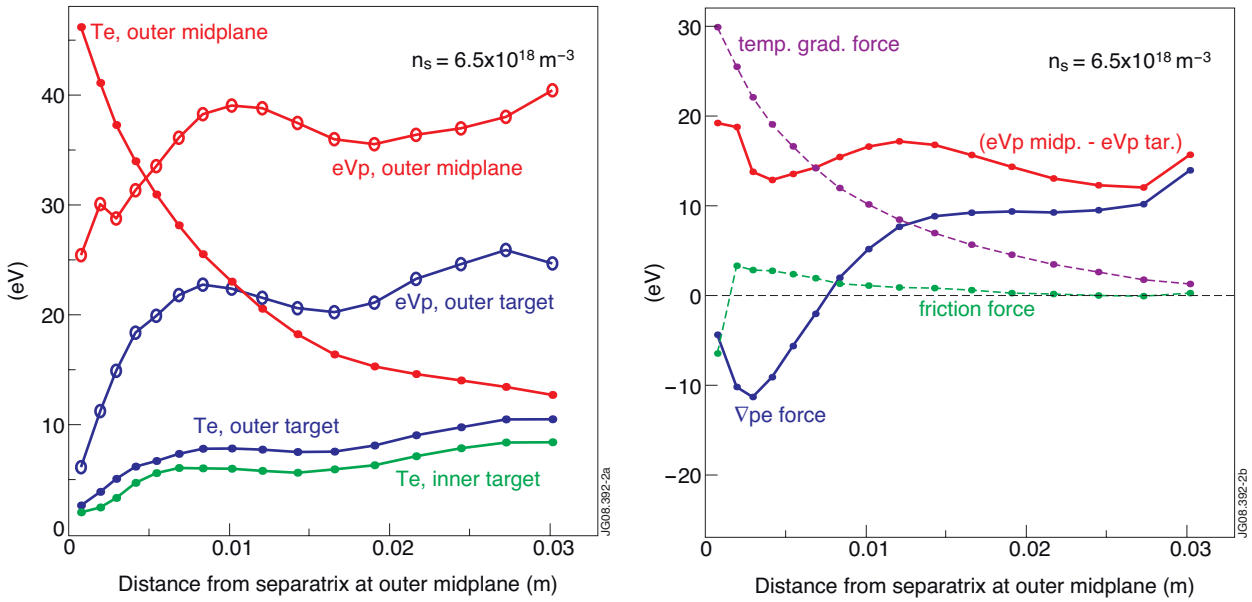

Figure 2: Same data as shown in Fig.1, but for the case with reversed B_t configuration.

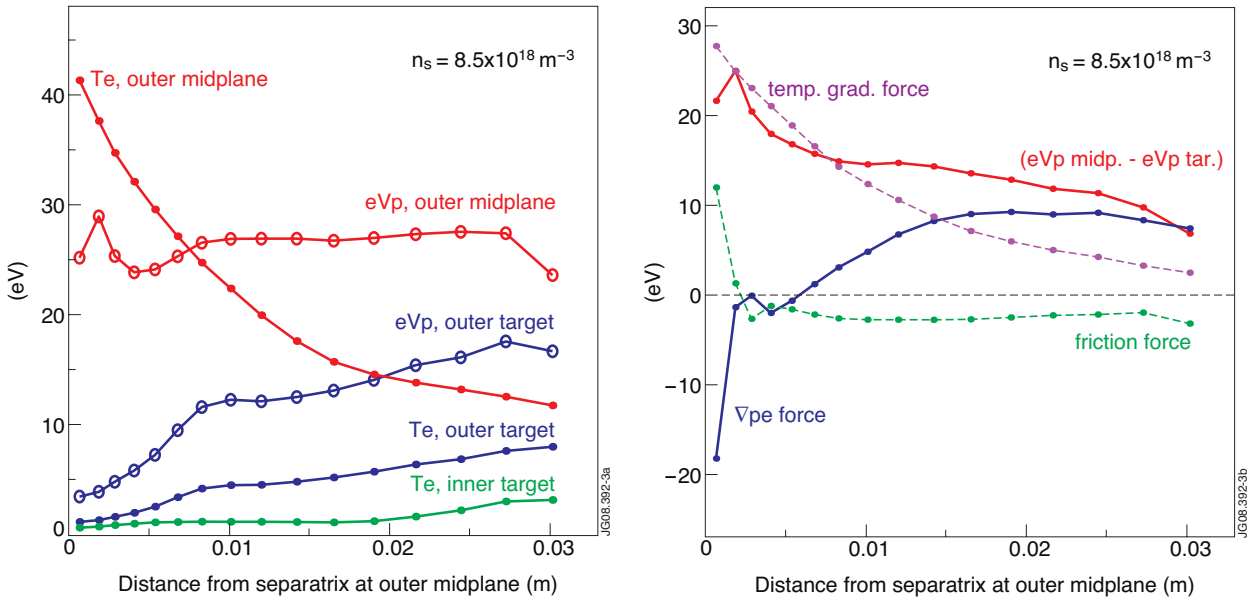

Figure 3: Same data as shown in Fig.1, but for the higher density Ohmic case, with $n_s = 8.5\times10^{18} m^{-3}$ (normal B_t configuration).

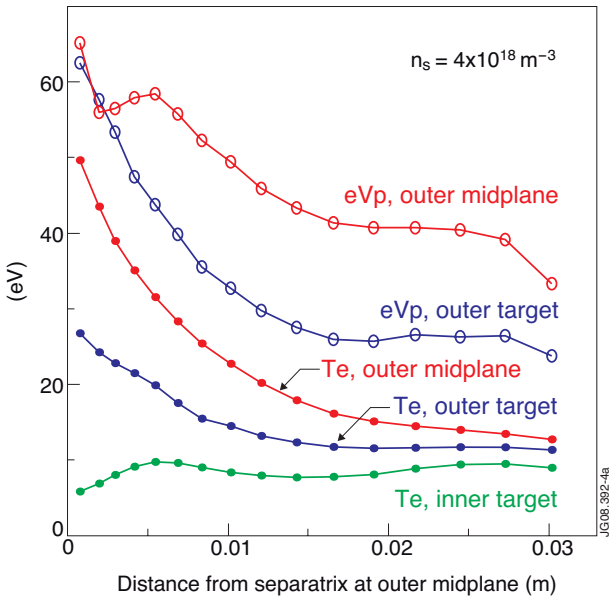

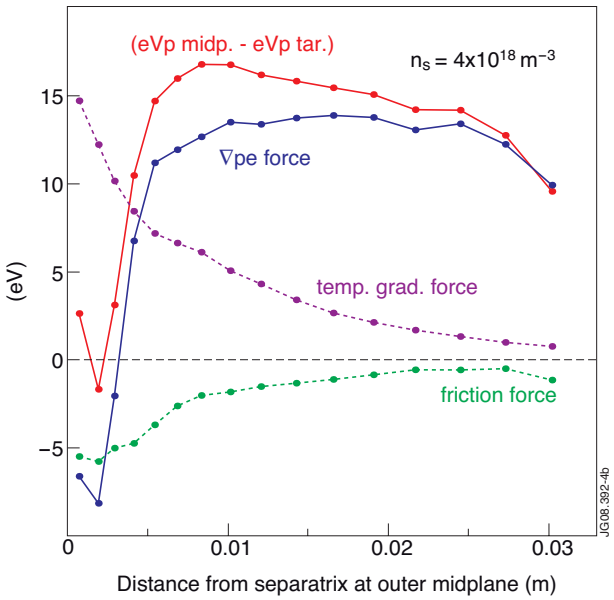

Figure 4: Same data as shown in Fig.1, but for the lower density Ohmic case, with $n_s = 4\times10^{18} m^{-3}$ (normal B_t configuration).

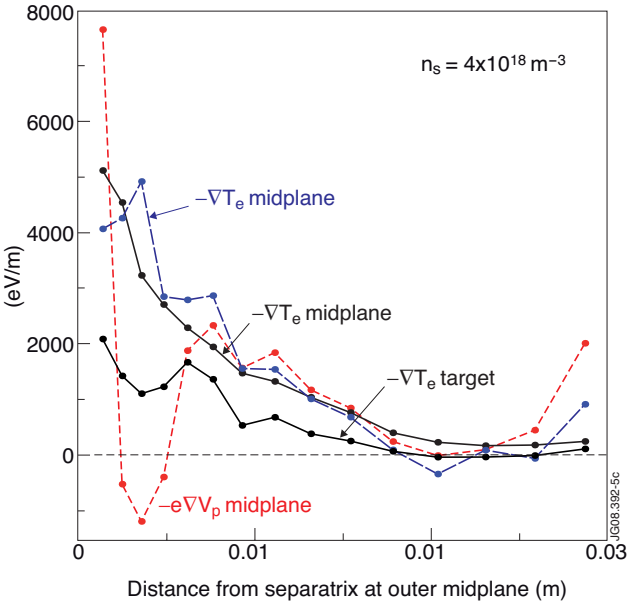

Figure 5: eE_r at outer target and midplane, $-\nabla T_e$ at outer target and midplane, for the Ohmic case, with $n_s = 4\times10^{18} m^{-3}$ (normal B_t configuration), shown in Fig. 4.

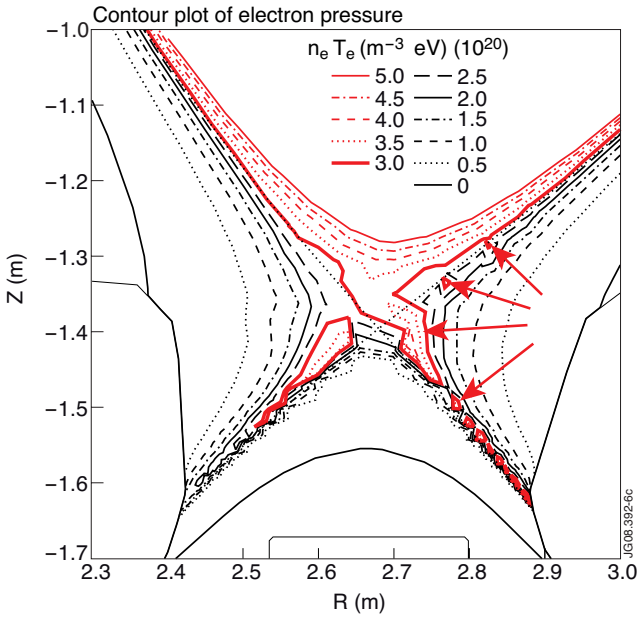

Figure 6: Contour plot of electron pressure for the case shown in Fig.4. The level $3\times10^{20}\ m^{-3}$eV is marked by a thicker line. Some regions where p_e exceeds this level are shown by arrows.

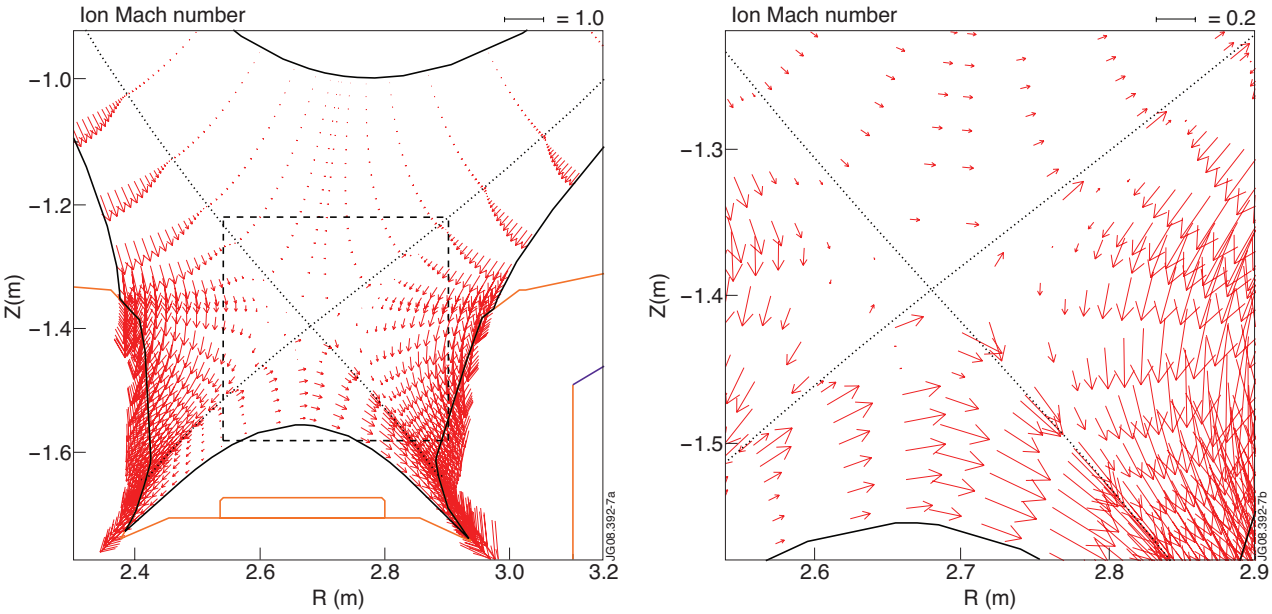

Figure 7: Vector plots of the parallel ion Mach number in and near the divertor, for the case shown in Fig.4. The close-up view (right) covers the area marked by dashed lines on the left figure.

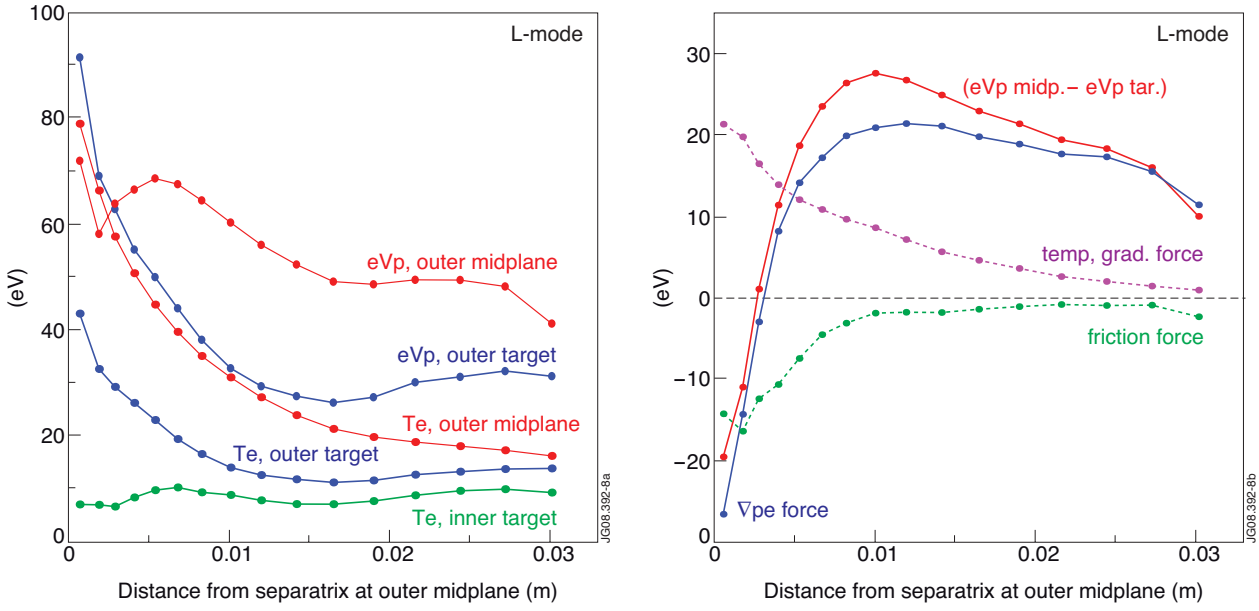

Figure 8: Same data as shown in Fig.1, but for the case with increased input power, 6MW, corresponding to the L-mode discharge, and $n_s = 5\times10^{18} m^{-3}$ (normal B_t configuration).